Journal of Biomechanics ∎ (∎∎∎∎) ∎∎∎–∎∎∎

Contents lists available at ScienceDirect

Journal of Biomechanics

journal homepage: www.elsevier.com/locate/jbiomech
www.JBiomech.com

Simulations of morphotype-dependent hemodynamics in non-dilated bicuspid aortic valve aortas

Kai Cao [a], Samantha K. Atkins [a], Andrew McNally [a], Janet Liu [b], Philippe Sucosky [b,*]

[a] Department of Aerospace and Mechanical Engineering, University of Notre Dame, Notre Dame, IN, USA
[b] Department of Mechanical and Materials Engineering, Wright State University, Dayton, OH, USA

ARTICLE INFO

Article history:
Accepted 2 November 2016

Keywords:
Bicuspid aortic valve
Aorta
Hemodynamics
Hemodynamic stress
Aortic disease

ABSTRACT

Bicuspid aortic valves (BAVs) generate flow abnormalities that may promote aortopathy. While positive helix fraction (PHF) index, flow angle (θ), flow displacement (d) and wall shear stress (WSS) exhibit abnormalities in dilated BAV aortas, it is unclear whether those anomalies stem from the abnormal valve anatomy or the dilated aorta. Therefore, the objective of this study was to quantify the early impact of different BAV morphotypes on aorta hemodynamics prior to dilation. Fluid-structure interaction models were designed to quantify standard peak-systolic flow metrics and temporal WSS characteristics in a realistic non-dilated aorta connected to functional tricuspid aortic valve (TAV) and type-I BAVs. While BAVs generated increased helicity (PHF > 0.68) in the middle ascending aorta (AA), larger systolic flow skewness ($\theta > 11.2°$) and displacement ($d > 6.8$ mm) relative to the TAV (PHF=0.51; $\theta < 5.5°$; $d < 3.3$ mm), no distinct pattern was observed between morphotypes. In contrast, WSS magnitude and directionality abnormalities were BAV morphotype- and site-dependent. Type-I BAVs subjected the AA convexity to peak-systolic WSS overloads (up to 1014% difference vs. TAV). While all BAVs increased WSS unidirectionality on the proximal AA relative to the TAV, the most significant abnormality was achieved by the BAV with left-right-coronary cusp fusion on the wall convexity (up to 0.26 decrease in oscillatory shear index vs. TAV). The results indicate the existence of strong hemodynamic abnormalities in non-dilated type-I BAV AAs, their colocalization with sites vulnerable to dilation and the superior specificity of WSS metrics over global hemodynamic metrics to the valve anatomy.

1. Introduction

The type-I bicuspid aortic valve (BAV) is the most common congenital cardiovascular defect and exists in different morphotypes, each with a distinct cusp fusion pattern (i.e., left-right-coronary cusp fusion (LR-BAV), right-non-coronary cusp fusion (RN-BAV) and non-left-coronary cusp fusion (NL-BAV)) (Ward, 2000). The BAV is a major risk factor for secondary aortopathy such as aortic dilation (Fedak et al., 2016; Michelena et al., 2011; Siu and Silversides, 2010), whose presentation depends on the BAV morphotype. While LR-BAVs are associated with aortic root dilation (type 1), RN- and NL-BAVs are more susceptible to dilation in the tubular portion of the ascending aorta (AA) (type 2) and in the proximal aortic arch (type 3) (Kang et al., 2013).

The dependence of the expression of aortopathy on the BAV subtype has suggested a role for hemodynamics in the etiology of BAV disease (Atkins and Sucosky, 2014). Flow eccentricity, skewness, helicity and wall shear stress (WSS) have been shown to be systematically higher in BAV aortas than in tricuspid aortic valve (TAV) aortas and to exhibit abnormalities in dilated BAV aorta regions (Barker et al., 2012; Bissell et al., 2013; Bonomi et al., 2015; Burris and Hope, 2015; Chandra et al., 2012; Mahadevia et al., 2014; Pasta et al., 2013; Seaman et al., 2014; van Ooij et al., 2015). While all these flow abnormalities may play different roles in BAV disease, they all impact the tissue via the interfacial fluid shear stress imposed on the endothelium. This observation combined with the established ability of vascular endothelial cells to sense and respond to changes in WSS magnitude, directionality and frequency through biological expression of cytokines, modulation of ion channels and smooth muscle cell signaling (Chiu and Chien, 2011; Lieu et al., 2004; Passerini et al., 2003) have suggested the key role played by WSS in BAV disease (Atkins et al., 2016a, 2016b). Despite the compelling evidence for the involvement of local flow abnormalities in the pathogenesis of BAV aortopathy, the existence of a

* Correspondence to: Department of Mechanical and Materials Engineering, Wright State University, 3640 Colonel Glenn Hwy, 257 Russ Engineering Center, Dayton, OH 45435, USA. Fax: +937 775 5082.
E-mail address: philippe.sucosky@wright.edu (P. Sucosky).

http://dx.doi.org/10.1016/j.jbiomech.2016.11.024
0021-9290/

hemodynamic etiology is still questionable as it is uncertain whether the reported flow abnormalities were due primarily to the valve morphology, the pre-existence of dilation in BAV patients, or anatomic differences between different patient cohorts. Addressing this uncertainty and isolating the early impact of the BAV anatomy on aortic flow require a controlled environment consisting of the same non-dilated aorta subjected to the flows of different BAV morphotypes. The present study aimed at addressing this need by examining computationally the early impact (i.e., prior to dilation) of different BAV morphotypes on the regional and temporal hemodynamic characteristics in a non-dilated aorta.

2. Materials and methods

2.1. Valve-aorta geometries

The three-dimensional valve-aorta geometry was designed in SolidWorks (Dassault Systemes, Inc) and consisted of the aortic root and the aorta (Fig. 1). The non-dilated aorta was reconstructed from a series of computed tomography images of a human aorta (Atkins et al., 2014; Cao and Sucosky, 2015) and consisted of the AA and the aortic arch along with brachiocephalic (BCA), left common carotid (LCCA) and left subclavian (LSCA) arteries. Consistent with our previous valve models (Cao et al., 2015; Cao and Sucosky, 2016), the TAV geometry consisted of three identical leaflets. Dimensional parameters for the aortic sinus and leaflets were obtained from published human aortic valve data (Thubrikar, 1989). The LR-BAV was constructed with a normal non-coronary leaflet and a larger leaflet mimicking fusion of the two coronary leaflets., The non-coronary leaflet and its sinus were designed to span a circumferential angle of 150° (Angelini et al., 1989; Sievers and Schmidtke, 2007). The left- and right-coronary leaflets were assumed to be identical and the raphe (i.e., line of fusion) was placed along the common free edge of these two leaflets. The RN-BAV and NL-BAV anatomies were obtained by rotating the entire LR-BAV valve apparatus (i.e., aortic root, aortic sinuses and leaflets) by 120° and 240°, respectively, about its axis.

2.2. FSI approach

The aortic wall and lumen were meshed with tetrahedral elements. In an effort to limit the computing time despite the large computational domain, the mesh strategy consisted of a coarser grid in the valvular flow region to generate qualitatively accurate flow patterns, and a finer grid with boundary layer treatment in the AA flow region where the WSS was to be analyzed. In addition, the structural domain was discretized using a coarser mesh than in the fluid domain since the focus of the study was on the flow characterization. Following a mesh sensitivity analysis, the final computational grid consisted of 70,000 elements in the structural domain (45,000 cells for the aorta and 25,000 cells for the aortic root and leaflets) and 1,014,000 elements in the fluid domain (632,000 cells in the aorta region and 382,000 cells in the valve region). This level of refinement achieved a spatial resolution of 80 μm near the aortic wall and generated only a 2% increase in peak-systolic WSS on the aortic wall relative to a mesh consisting of 25% smaller elements. Due to the implementation of an ALE FSI scheme, the mesh was automatically regenerated at time steps resulting in large structural deformations. The boundary layer mesh refinement was performed automatically on the fluid mesh generated at each time step. Fully coupled, two-way FSI simulations were performed in ANSYS 15.0 (ANSYS Inc.) using an arbitrary Lagrangian–Eulerian approach (Donea et al., 1982). The governing equations consisted of the momentum and continuity equations for the fluid domain, the momentum equation for the structure, and three coupling conditions enforcing continuity of displacements, velocities and tractions at the fluid-structure interface. The Navier–Stokes and continuity equations were solved using a finite volume method. The implicit flow solver used a second-order upwind spatial discretization scheme and a second-order temporal discretization scheme. The structural solver employed an implicit direct displacement-based finite element method. The system of equations was solved using the sparse direct solver and the equilibrium equations were solved by the Newton–Raphson method. A time step of 0.5 ms was implemented to discretize the entire cardiac cycle (0.86 s) and the simulations were run over three cardiac cycles to achieve temporal convergence.

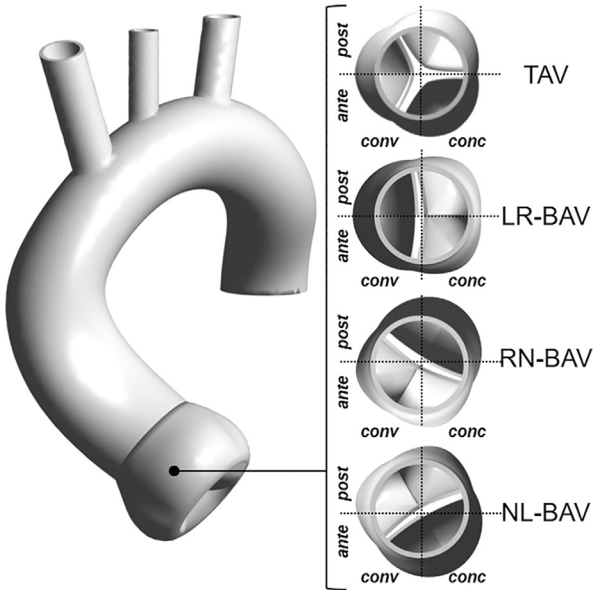

Fig. 1. Valve-aorta model and valve geometries (conv: convexity, conc: concavity, ante: anterior, post: posterior).

2.3. Material formulations and boundary conditions

The leaflet hyperelastic material was modeled using a previously published three-parameter incompressible Mooney–Rivlin model calibrated with respect to tensile test data on porcine leaflets (Cao et al., 2015). Consistent with previous artery and aorta models (Bathe and Kamm, 1999), the aortic wall was approximated as a linear, elastic, isotropic and nearly incompressible material (elastic modulus: 2 MPa; Poisson's ratio: 0.45). Blood was modeled as an incompressible, homogeneous and Newtonian fluid (density: 1050 kg/m^3; dynamic viscosity: 0.0035 Pa s). This approximation has been shown to generate less than 6% error in the predicted WSS on the leaflet fibrosa (i.e., low WSS region) relative to a non-Newtonian power-law model (Cao et al., 2015; Cao and Sucosky, 2016). The inlet boundary condition of the fluid domain consisted of a physiologic ventricular pressure waveform (0/120 mmHg, 2:1 diastolic/systolic ratio) and the four outlets of the aorta model (BCA, LCCA, LSCA and descending aorta) consisted of physiologic pressure waveforms obtained from the literature (Olufsen et al., 2000). The aortic wall was constrained in the axial direction at the inlet and outlet sections but was allowed to move in the radial and circumferential directions at all locations. A linear elastic support condition with a foundation stiffness of 75 mmHg/mm was prescribed on the outer aortic wall to simulate the damping effect generated by the surrounding tissues (Lantz et al., 2011). The implementation of the ALE strategy required a small 100-μm gap to be maintained between the leaflets in the coapted state. Frictionless conditions were prescribed between adjacent leaflets to simulate leaflet contact during coaptation. These conditions conditionally prevented leakage flow through the gap and treated the leaflets as in contact when the distance between two leaflets became smaller than 100 μm.

2.4. Flow characterization

Global aorta hemodynamics was assessed during the acceleration phase (t=70 ms), at peak systole (t=160 ms) and during the deceleration phase (t=240 ms) in terms of streamline, velocity and out-of-plane vorticity fields. All other flow characteristics were captured at common dilation sites for BAV aortas (Fig. 2A): 10 mm downstream of the sinotubular junction (proximal section, LR-BAV dilation) and 35 mm downstream of the sinotubular junction (middle section, NL-/RN-BAV dilation) (Agozzino et al., 2002; Evangelista et al., 2010). Flow helicity (Fig. 2B) was quantified in terms of the positive helix fraction (PHF) index (Faggiano et al., 2013),

$$\mathrm{PHF} = \frac{H_{pos}}{H_{pos} + H_{neg}}, \tag{1}$$

where H_{pos} and H_{neg} are the positive and negative parts, respectively, of the helicity flux over a section calculated as:

$$H = \int_S (\nabla \times ((\mathbf{V} \cdot \hat{\mathbf{t}})\hat{\mathbf{t}})) \cdot \hat{\mathbf{n}}\, dS \tag{2}$$

($\mathbf{V}$: velocity vector, $\hat{\mathbf{t}}$: unit vector tangent to the section, $\hat{\mathbf{n}}$: unit vector normal to the section, dS: surface element). The PHF represents the ratio of right-handed flows to the total helical flows over a section (PHF=0: purely left-handed helical flow; PHF=1: purely right-handed helical flow). Valvular jet skewness and eccentricity were quantified in terms of the flow angle θ (i.e., angle between the mean flow vector and the unit vector normal to the section of interest (Mahadevia et al., 2014); Fig. 2C), and flow displacement d (i.e., distance between the center of the section of interest and the centroid of the top 15% of velocities in the same section (Sigovan et al., 2011); Fig. 2D), respectively. The longitudinal (i.e., streamwise) WSS τ was captured at 20 points along the wall circumference in the proximal and middle AA

Please cite this article as: Cao, K., et al., Simulations of morphotype-dependent hemodynamics in non-dilated bicuspid aortic valve aortas. Journal of Biomechanics (2016), http://dx.doi.org/10.1016/j.jbiomech.2016.11.024